Title
Origins of Endo Selectivity in Diels–Alder Reactions of Cyclic Allene Dienophiles

Journal
Angewandte Chemie International Edition, 60(27)

ISSN
1433-7851

Authors
Ramirez, Melissa
Svatunek, Dennis
Liu, Fang
et al.

Publication Date
2021-06-25

DOI
10.1002/anie.202101809

Peer reviewed

HHS Public Access

Author manuscript

Angew Chem Int Ed Engl. Author manuscript; available in PMC 2022 June 25.

Published in final edited form as:

Angew Chem Int Ed Engl. 2021 June 25; 60(27): 14989–14997. doi:10.1002/anie.202101809.

Origins of *Endo* Selectivity in Diels–Alder Reactions of Cyclic Allene Dienophiles

Melissa Ramirez,
Department of Chemistry and Biochemistry, University of California, Los Angeles, Los Angeles, Ca 90095 (USA)

Dennis Svatunek,
Department of Chemistry and Biochemistry, University of California, Los Angeles, Los Angeles, Ca 90095 (USA)

Fang Liu,
College of Sciences, Nanjing Agricultural University, Nanjing 210095, China

Neil K. Garg,
Department of Chemistry and Biochemistry, University of California, Los Angeles, Los Angeles, Ca 90095 (USA)

K. N. Houk
Department of Chemistry and Biochemistry, University of California, Los Angeles, Los Angeles, Ca 90095 (USA)

Abstract

Strained cyclic allenes, first discovered in 1966 by Wittig and coworkers, have recently emerged as valuable synthetic building blocks. Previous experimental investigations, and computations reported here, demonstrate that the Diels–Alder reactions of furans and pyrroles to 1,2-cyclohexadiene and oxa and aza heterocyclic analogs proceed with *endo* selectivity. This unprecedented *endo* selectivity gives the adduct with the allylic saturated carbon of the cyclic allene *endo* to the diene carbons. The selectivity is very general and useful in synthetic applications. Our computational study establishes the origins of this *endo* selectivity. We analyze the helical frontier molecular orbitals of strained cyclic allenes and show how secondary orbital and electrostatic effects influence stereoselectivity. The LUMO of carbon-3 of the allene (C-3 is not involved in primary orbital interactions) interacts in a stabilizing fashion with the HOMO of the diene in such a way that the carbon of the cyclic allene attached to C-1 favors the *endo* position in the transition state. The furan LUMO, allene HOMO interaction reinforces this preference. These mechanistic studies are expected to prompt the further use of long-avoided strained cyclic allenes in chemical synthesis.

Graphical Abstract

A study of the factors contributing to *endo* selectivity in Diels–Alder reactions with strained cyclic allenes is reported. The contributions of a new type of secondary orbital interaction resulting from

neilgarg@chem.ucla.edu, houk@chem.ucla.edu, acialiu@njau.edu.cn.

the twisted nature of the strained allene, and electrostatic effects, to *endo* selectivity are established.

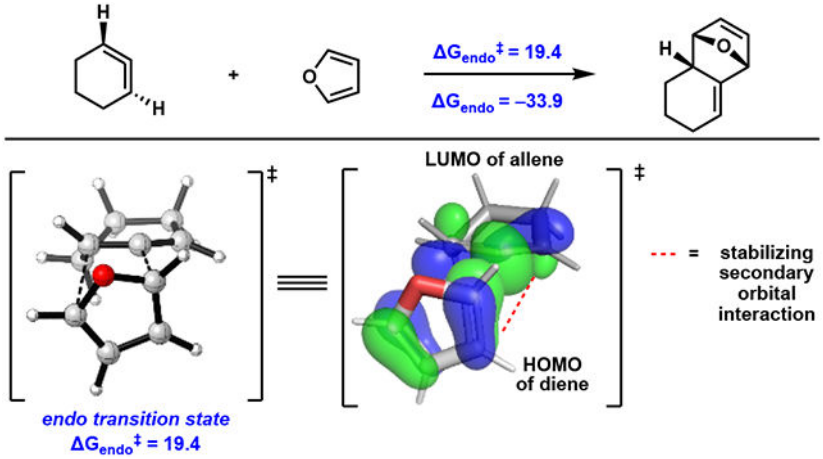

Keywords

cyclic allenes; cycloadditions; density functional theory; diastereoselectivity; substituent effects

Introduction

Strained cyclic allenes are valuable building blocks for the construction of complex molecular scaffolds.[1, 2] A recent application by the Schreiber group to create a DNA-encoded library synthesis exemplifies their utility.[2a] A diverse range of stereochemically-rich products can be accessed via highly *endo* selective Diels–Alder cycloadditions to strained cyclic allenes, as shown by cycloadducts **1**–**4** (Figure 1a).[2b-2e] Our groups[2c,d,f-i] and others[2j,k] have generated strained cyclic allenes from silyl triflates, **5**, and have found that *in situ* generated heterocyclic allenes, such as unsubstituted allenes **7** and **8**, participate in highly *endo* selective Diels–Alder reactions to provide adducts **13**–**22** (Figure 1b).[2c,d]

The simplest example of this *endo* selectivity is the cycloaddition of cyclohexa-1,2-diene (**25**) with furan (**24**) (Figure 1c).[2k] The reaction yields cycloadduct **26** in 80% yield with a 11:1 *endo*:*exo* ratio. Notably, there are no obvious secondary orbital interactions with unsaturated substituents attached to the reacting alkene, the usual feature that distinguishes an *endo* approach of a diene to a dienophile with extended unsaturation. Ordinarily, the preference for the *endo* Diels–Alder reaction arises from secondary interactions involving unsaturated substituents on the dienophile double bond, often polar activating groups such as an ester. *Endo* selectivity here refers to a CH_2 group of the cyclohexadiene (Figure 1c) oriented *cis* to the diene, and this lacks any unsaturation. The only analogous *endo* selectivity of a saturated group is the reactivity of dienes with cyclopropene, that exhibits high *endo* selectivity.[3] That case is known to arise from the very large hyperconjugation of the CH_2 of cyclopropene, but we show here that the explanation for cyclic allenes is entirely different.

Previous computational studies of *endo* and *exo* selectivities in Diels–Alder reactions involving strained dienophiles such as cyclopropenes, methylenecyclopropane, and derivatives thereof implicate the role of secondary orbital, electrostatic, and steric factors in *exo*/*endo* stereoselectivity.[3, 4] Acyclic allenes can participate in *endo* selective Diels–Alder reactions as well, but this selectivity is only achieved in cases where an ester substituent is present and a Lewis acid is used.[5] These studies cannot be directly applied to *endo* selectivity in reactions with cyclohexa-1,2-diene (**25**), which lacks such unsaturated substituents.

When an ester is attached to a reactive cyclic allene double bond, the ester is *exo* in products, while the saturated ring CH_2 is *endo* (see **19**–**22** above). A recent report by West provides many examples of *endo* cycloadditions of this type, in which unsaturated groups, CN and COR, are forced into an *exo* position.[2l] Previous computational investigations of Diels–Alder reactions of cyclic allenes[8] have not discussed *endo* selectivity, while West describes electrostatic interactions between the oxygen of furan (**24**) and a cyano group on the allene that stabilize the *exo-CN* transition, *endo*-cyclohexene transition state. This kind of interaction is not known to operate in normal Diels-Alder reactions of acrylonitrile. While we discuss such cases, our major goal was to understand why the CH_2 group invariably is *endo* in the favored transition state (Figure 1b).

We previously studied the reaction mechanism for the Diels–Alder reaction of cyclohexa-1,2-diene (**25**) with furan (**24**) at the (U)B3LYP/6-31G(d) level of theory.[2n] At that computational level, we proposed that the reaction proceeds via a stepwise, diradical mechanism with favored formation of the *endo* adduct, but did not explore the origins of the *endo* selectivity. Our more recent investigation on the Diels–Alder reaction of substituted azacyclohexa-3,4-dienes with the more accurate functional, ωB97X-D,[6] shows that these reactions occur instead by a highly asynchronous, but concerted, Diels–Alder mechanism.[2c] These calculations were consistent with experimentally observed *endo* selectivities, but no attempts were made at that time to analyze the factors leading to this *endo* selectivity.

Results and Discussion

Molecular Orbital Analysis of Cyclohexa-1,2-diene (25)

Previous computational studies have provided an examination of the electronic structure of cyclic allenes and, in some cases, a comparison to that of linear allenes.[7] Bickelhaupt, Hamlin, *et al.* have extensively analyzed the regioselectivity of 1,3-dipolar cycloadditions of linear and bent substituted allenes and concluded that orbital interactions control reactivity and regioselectivity.[7f] We provide an orbital interaction analysis of a related, but entirely different phenomenon here, the stereoselectivity of Diels-Alder cycloadditions of cyclic allenes. We begin by describing the π MOs of linear and cyclic allenes and the interactions of diene orbitals with these allene π orbitals to explain the origins of stereoselectivity in their Diels–Alder reactions.

We first analyzed the electronic structure of the linear allene 2,3-pentadiene (**27**) and compared it to that of cyclohexa-1,2-diene (**25**). Computations were performed using Gaussian 16. Geometry optimizations were carried out using the ωB97X-D functional[6] and

the 6-311+G(d,p) basis set. Energy minima were verified through vibrational analysis. Molecular orbitals and orbital energies were calculated using HF/6-31G(d). Similar conclusions can be made based upon Kohn-Sham orbitals at the ωB97X-D/6-31G(d) level. Molecular orbitals are illustrated using PyMol 2.4.0. Figure 2a shows the computed frontier molecular orbitals (FMOs) of 2,3-pentadiene (**27**). The degenerate HOMOs and LUMOs of **27** have helical topologies,[8] and can be represented by the combination of localized orthogonal **π** and **π*** orbitals, respectively. The HOMO–a and LUMO–a of **27** are left-handed helices, whereas the HOMO–b and LUMO–b are right-handed helices. It has been proposed that a slight split in degeneracy occurs in 2,3-pentadiene (**27**) due to the reduction of symmetry from the D_{2d} symmetry of the allene.[8a]

A significant degree of distortion is required to constrain the allene into a six-membered ring such that the aforementioned representation of the MOs as involving only orthogonal p orbitals is no longer suitable for understanding the MOs of cyclic allene **25** and their involvement in [4+2] cycloadditions. As a result of twisting and bending the allene (i.e., altering the bond angle formed by the three allenic carbon atoms from 180° to 133°), the FMOs of cyclohexa-1,2-diene (**25**) also become significantly non-degenerate (Figure 3). The energies of the LUMO (2.9 eV) and LUMO+1 (5.9 eV) differ by 2.9 eV whereas the HOMO (−8.5 eV) and HOMO–1 (−10.0 eV) are non-degenerate by 1.5 eV. In addition, allene bending results in increased s-character at C2 of the LUMO of **25**.

Figure 3 shows how the FMOs can be constructed from two distorted and twisted localized **π** and **π*** orbitals of two ethylenes in an allene. The two bonding MOs, prior to mixing, are depicted as $\boldsymbol{\pi}_1$ and $\boldsymbol{\pi}_2$. Bending at the allene central carbon gives s orbital admixture with the p orbital (towards sp^2). Combination of the p orbitals at the central carbon provides tilted p orbitals that overlap with the terminal hybrid orbitals. Additive and subtractive combinations of the bonding MOs $\boldsymbol{\pi}_1$ and $\boldsymbol{\pi}_2$ provide the HOMO and HOMO–1 of cyclohexa-1,2-diene (**25**), respectively. Because they interact, they are stabilized and destabilized and no longer remain degenerate. The antibonding MOs of cyclohexa-1,2-diene (**25**) can be described similarly. Prior to mixing, the antibonding MOs can be represented as $\boldsymbol{\pi}_1^*$ and $\boldsymbol{\pi}_2^*$. Additive and subtractive combinations of $\boldsymbol{\pi}_1^*$ and $\boldsymbol{\pi}_2^*$ provides the LUMO and LUMO+1 of cyclohexa-1,2-diene (**25**), respectively. The LUMO of **25** has a larger MO coefficient at C2 and, as such, Diels–Alder reactions with electron-rich dienes (e.g. furan) are expected to occur with preferential bonding at C2 of cyclohexa-1,2-diene (**25**).

Transition States of the [4+2] Cycloaddition Reaction of Cyclohexa-1,2-diene (25) with Furan (24), and Analysis of *Exo*/*Endo* Differences

The Gibbs energy barriers for the reaction of **25** with furan (**24**) to provide *endo* and *exo* adducts **26-endo** and **26-exo**, respectively, were calculated and are shown in Figure 4a. Calculations were performed as above. Solvation effects of tetrahydrofuran (THF) or acetonitrile (MeCN) were included using the solvation model SMD[9] with a standard state of 1 M. Energy minima and transition states were verified through vibrational analysis. Truhlar's quasiharmonic correction was applied by setting all positive frequencies below 100 cm^{-1} to 100 cm^{-1}.[10] Hirshfeld charges and electrostatic potential maps were obtained using ωB97X-D/6-311+G(d,p). Optimized structures and are illustrated using CYLview.[11]

Formation of *endo* adduct **26** is predicted to occur with an energy barrier of 19.4 kcal mol^{-1}. The *exo* transition state is 1.7 kcal mol^{-1} higher in energy than the *endo* transition state, which correlates well with experimental results (11:1 *endo*:*exo*). The *exo* and *endo* transition structures **TS-1-exo** and **TS-2-endo**, respectively, reveal the highly asynchronous nature of the cycloaddition (Figure 4b). **TS-1-exo** and **TS-2-endo** also show that orbital overlap of the HOMO of furan (**24**) with the p orbital on C2 of allene **25** is maximized in the *endo* approach of **24** to **25**. The *endo* reaction is slightly thermodynamically favored ($\Delta G = -33.9$ kcal mol^{-1}) over the *exo* reaction ($\Delta G = -32.7$ kcal mol^{-1}).

To understand the origin of this stereoselectivity, a distortion/interaction activation-strain (D/IAS) analysis was performed.[12,13] In a D/IAS analysis, activation potential energies ($\Delta E^{\ddagger}$) are analyzed. For each transition state, $\Delta E^{\ddagger}$ is further broken down into the distortion energy ($\Delta E_{dist}^{\ddagger}$) and the interaction energy ($\Delta E_{int}^{\ddagger}$). The $\Delta E_{dist}^{\ddagger}$ is the energetic cost of deforming the ground states of the reactants into their transition state geometries. The $\Delta E_{int}^{\ddagger}$ is an energetic benefit resulting from stabilizing electronic interactions between fragments in the transition state. As shown in Figure 4c, $\Delta E_{dist}^{\ddagger}$ is only slightly higher in the **TS-1-exo** ($\Delta\Delta E_{dist}^{\ddagger} = -0.3$ kcal mol^{-1}). $\Delta E_{int}^{\ddagger}$ was found to be significantly more stabilizing for **TS-2-endo** ($\Delta\Delta E_{int}^{\ddagger} = -1.5$ kcal mol^{-1}), indicating that the reaction is selective due to more stabilizing electronic interactions in **TS-2-endo** than in **TS-1-exo**.[14]

To better understand the favorable electronic interactions that lead to stabilization of ΔE_{int} along the *endo* reaction pathway, an energy decomposition analysis (EDA) was performed along both the *endo* and *exo* reaction coordinates. EDA was carried out using the ADF.2018.106 program[15,16] at the ωB97X-D/TZ2P level of theory on the geometries optimized at ωB97X-D/6-311+G(d,p)/SMD(THF) Gaussian 16. An EDA involves the decomposition of ΔE_{int} into electrostatic (ΔV_{elstat}), Pauli repulsive (ΔE_{Pauli}), and orbital interactions (ΔE_{orb}) as shown in Equation 1.

$$\Delta E_{int} = \Delta V_{elstat} + \Delta E_{Pauli} + \Delta E_{orb} \quad \text{(Eq. 1)}$$

ΔV_{elstat} accounts for the electrostatic interaction between the deformed reactants, ΔE_{Pauli} accounts for the destabilizing interactions between occupied orbitals (i.e., steric repulsion), and ΔE_{orb} represents the degree of charge transfer between the two reactants (e.g., HOMO–LUMO interactions or polarization). In Figure 5, the EDA terms for *endo* and *exo* pathways are plotted along the reaction coordinate. The x-axis corresponds to the length of the forming bond to the central carbon of the allene unit in cyclohexa-1,2-diene (**25**). ΔE_{Pauli} is slightly less destabilizing in the *exo* reaction pathway, which is likely due to the longer lengths of the forming bonds and thus, a smaller degree of steric repulsion. In contrast, ΔE_{orb} and ΔV_{elstat} are more favorable in the *endo* reaction pathway and account for the more stabilizing ΔE_{int} associated with formation of *endo* product **26-endo**. Thus, the EDA analysis provides evidence that orbital and electrostatic interactions enable more stabilizing ΔE_{int} in the formation of *endo* product **26-endo**.

To explain why ΔE_{orb} favors the *endo* transition state, we analyzed the FMO interactions in **TS-2-endo** and **TS-1-exo** (Figure 5). The MOs of the allene LUMO and diene HOMO at

TS-2-endo and **TS-1-exo** were calculated at the TS geometry with HF/6-311+G(d,p). There is a secondary orbital interaction that stabilizes **TS-2-endo** and has little effect on **TS-1-exo**. Figure 6 shows two perspectives of **TS-2-endo** and **TS-1-exo** that highlight this secondary orbital interaction.

The interactions are shown from two different perspectives in Figure 6a and 6b. The stabilizing secondary orbital interaction in **TS-2-endo** involves orbital overlap of the HOMO at C3' of furan (**24**) with the LUMO at C3 of cyclohexa-1,2-diene (**25**). In **TS-1-exo**, the orbital at C3' of furan (**24**) is out-of-phase with the LUMO of C3 of allene **25** and, therefore, cannot engage in stabilizing interactions. The stabilizing interaction in **TS-2-endo** is indeed related to the secondary orbital interaction that stabilizes more conventional Diels-Alder transition states, like butadiene or cyclopentadiene dimerization, but occurs here only because of the twisting of the LUMO of the distorted allene. It does not operate in acyclic linear allenes.

Orbital interactions in the *endo* and *exo* reaction pathways were quantified using extended transition state-natural orbitals for chemical valence (ETS-NOCV). ETS-NOCV analyses were carried out using the ADF.2018.106 program[15,16] at the ωB97X-D/TZ2P level of theory on the geometries optimized at the ωB97X-D/6-311+G(d,p)/SMD(THF) level in Gaussian 16. Results from ETS-NOCV along the *endo* and *exo* reaction coordinates are shown in Figure 7a. The x-axis corresponds to reaction progress or the C—C bond forming distance to the central carbon of the allene. The strongest interaction (interaction A in Figure 7a) arises from overlap between allene (**25**) LUMO and furan (**24**) HOMO and favors the *endo* reaction. The second strongest ETS-NOCV interaction, interaction B, is due to overlap between the allene **25** HOMO and furan (**24**) LUMO and is also stronger in the *endo* transition state. Thus, results from ETS-NOCV reveal that in both normal and inverse electron-demand Diels–Alder reactions of **24** and **25**, orbital interactions are more stabilizing along the *endo* pathway.

Although the allene **25** LUMO/furan (**24**) HOMO energy gap (11.8 eV, Figure 7b) is smaller than that of the allene **25** HOMO/furan (**24**) LUMO pair (12.9 eV), orbital interactions between the allene **25** HOMO and furan (**24**) LUMO still contribute to *endo* selectivity. This is supported by results from the EDA, which shows that orbital overlap between the allene **25** HOMO and furan (**25**) LUMO is greater along the *endo* pathway than along the *exo* pathway (Figure 8a). Thus, results from the ETS-NOCV method and EDA reveal the presence of a favorable allene **25** HOMO/furan (**24**) LUMO interaction in the *endo* TS that further contribute to stereoselectivity. This interaction is shown in Figure 8b and involves overlap of the LUMO at C3' of furan (**24**) with the HOMO at C3 of allene **25**.

As mentioned earlier, results from the EDA demonstrated that ΔV_{elstat} is also more favorable in the *endo* reaction pathway. Thus, we analyzed the ΔV_{elstat} term that contributes to ΔE_{int} and the *endo* selectivity by comparing electrostatic interactions in the *endo* and *exo* reaction pathways. Electrostatic charges are most comparable at analogous geometries along the reaction coordinate where the same degree of bond formation has occurred. Since the *endo* TS occurs earlier than the *exo* TS ($\Delta E_{endo}^{\ddagger}$ = 5.6 kcal mol^{-1} while $\Delta E_{exo}^{\ddagger}$ = 7.3 kcal mol^{-1}), it was necessary to first identify analogous geometries along each reaction pathway and then

calculate electrostatic charges of the corresponding structures. We chose analogous *endo* and *exo* geometries where C—C bond forming distances to the central carbon of the allene are very similar (2.25–2.26 Å).

Figure 9 shows the analogous geometries **Endo Structure A** (ΔE = 4.9 kcal mol^{-1}) and **Exo Structure B** (ΔE = 6.2 kcal mol^{-1}). It also summarizes the Hirshfeld charges of the oxygen atom of furan (**24**) and the allenic protons H1 or H3 (see the Supporting Information Part II for Hirshfeld charges of additional atoms) and shows the corresponding electrostatic potential maps. In **Endo Structure A**, the oxygen atom of **24** and H1 of allene **25** are in closer proximity (2.8 Å) than are the oxygen atom of **24** and H3 in **Exo Structure B** (3.6 Å). There is a stabilizing electrostatic interaction and stabilization in the *endo* reaction pathway, which is further supported by the electrostatic potential map of **Endo Structure A**. The reduced *endo* selectivity calculated for the reaction of cyclohexa-1,2-diene (**25**) with cyclopentadiene, which lacks the partially negative oxygen, also serves as evidence for this.[17] The electrostatic potential maps also show that the **Exo Structure B** is destabilized by a repulsive H2'-H3 interaction that is much smaller in **Endo Structure A**. Overall, our analysis reveals the electrostatic and orbital interactions that allow for *endo* selectivity in the Diels–Alder reaction of cyclohexa-1,2-diene (**25**) and furan (**24**). Secondary orbital interactions stabilize the *endo* approach of diene **24** to allene **25** and involve orbital overlap of the HOMO at C3' of diene **24** with the LUMO at C3 of allene **25**.

Diels–Alder Reactions of Strained Heterocyclic Allenes

We have also computed the *endo*/*exo* selectivity in Diels–Alder cycloadditions with other strained heterocyclic allenes and dienes (Figure 10). The Gibbs energy barriers ($\Delta G^{\ddagger}$) for Diels–Alder reactions of allenes **7**, **29**, and **31** with dienes **24**, **28**, or **34** were computed (Figure 10).[18] Previous experimental studies demonstrated that Diels–Alder reactions of allenes **7**, **29**, and **31** proceed with good to excellent *endo* selectivity (7.4:1 to >20:1 *endo*:*exo*, Figure 10).[2c, 2d] Interestingly, methyl-substituted allene **31** undergoes the [4+2] cycloaddition with higher stereoselectivity (>20:1 *endo*:*exo*) than unsubstituted allenes **7** and **29**. Computational analysis of the reaction with **31** in comparison to the reactions with allenes **7** and **29** were undertaken to provide insight into allene substituent effects on *endo* selectivity in Diels-–Alder reactions with strained cyclic allenes.

The calculations on cycloadditions of oxacyclic allene **7** with 2,5-dimethylfuran (**28**) and azacyclic allene **29** and furan (**24**) indicate that formation of *endo* adducts **13-endo** and **30-endo** proceed with barriers of $\Delta G^{\ddagger}$ = 17.4 kcal mol^{-1} and $\Delta G^{\ddagger}$ = 16.8 kcal mol^{-1}, respectively. Formation of *exo* adducts **13-exo** ($\Delta G^{\ddagger}$ = 19.5 kcal mol^{-1}) and **30-exo** ($\Delta G^{\ddagger}$ = 18.3 kcal mol^{-1}) is disfavored by 1.5–2.1 kcal mol^{-1}. Our calculated $\Delta\Delta G^{\ddagger}$ of 2.1 kcal mol^{-1} (35:1 *endo*:*exo* ratio) for reaction of allene **7** and 2,5-dimethylfuran (**28**) and 1.5 kcal mol^{-1} (13:1 *endo*:*exo* ratio) for reaction of allene **29** and furan (**24**) are in reasonable agreement with the experimental *endo*:*exo* ratios of 9.2:1 and 7.4:1, respectively.

Energetic barriers were also evaluated for the cycloadditions of alkyl-substituted allene **31** with furan (**24**), 2,5-dimethylfuran (**28**), and *N*-phenylpyrrole (**34**). Previous computational studies performed by our lab demonstrated that the alkyl substituent in allene **31** allows for

regioselective addition onto the more electron poor π bond of allene **31** via an electronic effect.[2c,19] Therefore, reaction pathways corresponding to regioselective addition onto the unsubstituted π bond of allene **31** were considered for the stereoselectivity studies shown in Figure 10. Our calculated $\Delta\Delta G^{\ddagger}$ values of 0.7–3.9 kcal mol^{-1} for the cycloadditions of allene **31** with dienes **24**, **28**, and **34** demonstrate that *endo* adducts **32-endo**, **33-endo**, and **35-endo** are generated preferentially over *exo* adducts **32-exo**, **33-exo**, and **35-exo**.[20] Computed $\Delta\Delta G^{\ddagger}$ values qualitatively agree with the experimental *endo*:*exo* ratios shown in Figure 10.

To gain insight regarding substituent effects on stereoselectivity, D/IAS analysis was performed for reactions of allene **29** with furan (**24**) and allene **31** with dienes **24**, **28**, and **34**. We hypothesized that hyperconjugative interactions of the allenic methyl substituent with the non-reactive π bond of **31** allows for stronger secondary orbital interaction between the diene and dienophile in the *endo* reaction. To provide support for our hypothesis, we performed a D/IAS analysis of the reaction of allene **31** with diene **24**. Based on the analysis, the comparatively higher *endo* selectivity in Diels–Alder reactions of allene **31** with **24** ($\Delta\Delta G^{\ddagger}$ = 3.2 kcal mol^{-1}) is attributed to both more stabilizing ΔE_{int} and lower ΔE_{dist} along the *endo* reaction pathway.[21] The more stabilizing ΔE_{int} supports the idea that hyperconjugative interactions allowing for stronger secondary orbital interactions in the *endo* reaction. Additionally, the lower ΔE_{dist} emerges from the presence of unfavorable steric interactions between the H at C2' of furan (**24**) and the methyl substituent on allene **31** along the *exo* reaction pathway.

D/IAS analysis for the reaction of allene **31** with 2,5-dimethylfuran (**28**) ($\Delta\Delta G^{\ddagger}$ = 3.9 kcal mol^{-1}) was performed next, revealing that the enhanced *endo* selectivity arises from steric, rather than electronic, factors.[21] In this case, the methyl group at C2' of 2,5-dimethylfuran (**28**) has unfavorable steric interactions with the methyl substituent in allene **31** in the *exo* approach of the diene to the dienophile. Interestingly, selectivity in the reaction of allene **31** with *N*-phenylpyrrole (**34**) decreases ($\Delta\Delta G^{\ddagger}$ = 0.7 kcal mol^{-1}) due to competing ΔE_{int} and ΔE_{dist} along *endo* and *exo* reaction coordinates. While ΔE_{dist} is lower in the *endo* reaction, *N*-phenylpyrrole (**34**) does not have as stabilizing secondary orbital interactions with allene **31** as does furan (**24**).[22] This may be due to differences in orbital localization in furans and pyrroles.

Conclusion

This study elucidates the factors contributing to *endo* selectivity in Diels–Alder reactions with strained cyclic allenes. In the *endo* reaction pathways of dienes with cyclohexa-1,2-diene and heterocyclic and substituted analogs, there is a stabilizing interaction between C3' (attached to the furan atom that is bonding to the central carbon of allene) and the LUMO orbital at C3 of the allene. The latter is a new type of secondary orbital interaction that results from the near perpendicular approach of the diene to the dienophile and the twisted nature of the strained allene. In the *exo* TS, this interaction is small but destabilizing. The attractive electrostatic interaction of the oxygen atom of furan (**24**) with the proximal allenic proton H1 of allene **25** provides additional stabilization in the *endo* reaction pathway. West proposed an electrostatic interaction of the furan O with an *exo* CH carbon.[21] We also studied the selectivities of Diels–Alder reactions of various dienes with heterocyclic allenes,

including oxacyclohexa-3,4-diene (**7**), azacyclohexa-3,4-diene (**29**), and 3-methyl-1-azacyclohexa-3,4-diene (**31**). Computed *endo* selectivities agreed with experimental results. These selectivities are generally 1–2 kcal mol^{-1}, larger than the well-known *endo* selectivities for monosubstituted dienophiles with cyclopentadiene (0.5–1 kcal mol^{-1}).[23] These results are expected to prove useful in future synthesis design involving Diels–Alder reactions with strained cyclic allenes.

Supplementary Material

Refer to Web version on PubMed Central for supplementary material.

Acknowledgements

The authors are grateful to the NIH NIGMS (R01 GM123299 and R01 GM132432 to N.K.G. and F31 GM130099-02 to M.R.), the National Science Foundation (CHE-1764328 to K.N.H.), the Austrian Science Fund (FWF, J 4216-N28 to D.S.), the City of Vienna (H-331849/2018 to D.S.), and the Natural Science Foundation of Jiangsu Province, China (BK20190505 to F. L.) for financial support of this research. This study used computational and storage services associated with the Hoffman2 Shared Cluster provided by the UCLA Institute for Digital Research and Education. Calculations were in part performed at the Vienna Scientific Cluster.

References

[1]. The parent cyclic allene, cyclohexa-1,2-diene, was first accessed by Wittig and coworkers, see: Wittig G, Fritze P, Angew. Chem., Int. Ed. Engl 1966, 5, 846.

[2]. (a)For synthetic methodologies involving cyclic allene chemistry, see: Westphal MV, Hudson L, Mason JW, Pradeilles JA, Zécri FJ, Briner K, Schreiber SL, J. Am. Chem. Soc 2020, 142, 7776–7782; [PubMed: 32267148] (b)Drinkuth S, Groetsch S, Peters E-M, Peters K, Christl M, Eur. J. Org. Chem 2001, 14, 2665–2670;(c)Barber JS, Yamano MM, Ramirez M, Darzi ER, Knapp RR, Liu F, Houk KN, Garg NK, Nat. Chem 2018, 10, 953–960; [PubMed: 30061614] (d)Yamano MM, Knapp RR, Ngamnithiporn A, Ramirez M, Houk KN, Stoltz BM, Garg NK, Angew. Chem., Int. Ed 2019, 58, 5653–5657;(e)Elliott RL, Nicholson NH, Peaker FE, Takle AK, Tyler JW, White J, J. Org. Chem 1994, 59, 1606–1607;(f)Barber JS, Styduhar ED, Pham HV, McMahon TC, Houk KN, Garg NK, J. Am. Chem. Soc 2016, 138, 2512–2515; [PubMed: 26854652] (g)Yamano MM, Kelleghan AV, Shao Q, Giroud M, Simmons BJ, Li B, Chen S, Houk KN, Garg NK, Nature, 2020, 586, 242–247; [PubMed: 32846425] (h)McVeigh MS, Kelleghan AV, Yamano MM, Knapp RR, Garg NK, Org. Lett 2020, 22, 4500–4504; [PubMed: 32437158] (i)Chari J, Ippoliti F, Garg NK, J. Org. Chem 2019, 84, 3652–3655; [PubMed: 30840455] (j)Guitián E, Peña D, Perez D, Quintana I, Eur. J. Org. Chem 2009, 5519–5524;(k)Lofstrand VA, West FG, Chem. Eur. J 2016, 22, 10763–10767; [PubMed: 27219685] (l)Wang B, Constantin MG-, Singh S, Zhou Y, Davis RL, West FG, Org. Biomol. Chem 2021, 19, 399–405; [PubMed: 33300539] (m)Almehmadi YA, West FG, Org. Lett 2020, 22, 6091–6095; [PubMed: 32790431] (n)Nendel M, Tolbert LM, Herring LE, Islam MN, Houk KN, J. Org. Chem 1999, 64, 976–983; [PubMed: 11674172] (o)Wentrup C, Gross G, Maquestiau A, Flammang R, Angew. Chem. Int. Ed. Engl 1983, 22, 542–543;(p)Schreck M, Christl M, Angew. Chem., Int. Ed 2017, 56, 10070–10086; (q)Christl M, Fischer H, Arnone M, Engels B, Chem. Eur. J 2009, 15, 11266–11272; [PubMed: 19746463] (r)Bottini AT, Hilton LL, Plott J, Tetrahedron 1975, 31, 1997–2001;(s)Lofstrand VA, McIntosh KC, Almehmadi YA, West FG, Org. Lett 2019, 21, 6231–6234; [PubMed: 31343882] (t)Elliott RL, Nicholson NH, Peaker FE, Takle AK, Richardson CM, Tyler JW, White J, Pearson MJ, Eggleston DS, Haltiwanger RS, J. Org. Chem. 1997, 62, 4998–5016;(u)Christl M, Drinkuth S, Eur. J. Org. Chem 1998, 237–241;(v)Christl M, Braun M, Fischer H, Groetsch S, Müller G, Leusser D, Deuerlein S, Stalke D, Arnone M, Engels B, Eur. J. Org. Chem 2006, 5045–5058; (w)Engels B, Schöneboom JC, Münster AF, Groetsch S, Christl M, J. Am. Chem. Soc 2002, 124, 287–297; [PubMed: 11782181] (x)Christl M, Braun M, Wolz E, Wagner W, Chem. Ber 1994, 127, 1137–1142.

[3]. Levandowski BJ, Houk KN, J. Am. Chem. Soc 2016, 138, 16731–16736. [PubMed: 27977194]

[4]. Levandowski BJ, Hamlin TA, Helgeson RC, Bickelhaupt FM, Houk KN, J. Org. Chem 2018, 83, 3164–3170. [PubMed: 29470085]

[5]. Ishar MPS, Wali A, Gandhi RP, J. Chem. Soc. Perkin Trans. 1 1990, 8, 2185–2192.

[6]. Chai J-D, Head-Gordon M, Phys. Chem. Chem. Phys 2008, 10, 6615–6620. [PubMed: 18989472]

[7]. (a)For previous computational studies of cyclic allenes that have provided analysis of their electronic structure, see: Dillon PW, Underwood GR, J. Am. Chem. Soc 1974, 96, 779–787. (b)Schmidt MW, Angus RO, Johnson RP, J. Am. Chem. Soc 1982, 104, 6838–6839.(c)Angus RO, Schmidt MW, Johnson RP, J. Am. Chem. Soc 1985, 107, 532–537.(d)Hänninen MM, Peuronen A, Tuononen HM, 2009, 15, 7287–7291.(e)Daoust KJ, Hernandez SM, Konrad KM, Mackie ID, Winstanley J, Johnson RP, J. Org. Chem 2006, 71, 5708–5714. [PubMed: 16839152] (f)Yu S, Vermeeren P, van Dommelen K, Bickelhaupt FM, Hamlin TA, Chem. Eur. J 2020, 26, 11529–11539. [PubMed: 32220086]

[8]. (a)Although the helical nature of strained cyclic allenes has not been studied, that of linear allenes has been, see: Hendon CH, Tiana D, Murray AT, Carbery DR, Walsh A, Chem. Sci 2013, 4, 4278–4284;(b)Garner MH, Hoffmann R, Rettrup S, Solomon GC, ACS Cent. Sci 2018, 4, 688–700. [PubMed: 29974064]

[9]. Marenich AV, Cramer CJ, Truhlar DG, J. Phys. Chem. B 2009, 113, 6378–6396. [PubMed: 19366259]

[10]. Ribeiro RF, Marenich AV, Cramer CJ, Truhlar DG, J. Phys. Chem. B 2011, 115, 14556–14562. [PubMed: 21875126]

[11]. Legault CY, CYLView, 1.0b; Université de Sherbrooke: Quebec, Montreal, Canada, http://www.cylview.org (2009).

[12]. Houk KN, Bickelhaupt FM, Angew. Chem., Int. Ed 2017, 56, 10070–10086.

[13]. (a)For additional applications of the distortion/interaction activation-strain model to reactions of cyclic alkynes and arynes, see: McMahon TC, Medina JM, Yang Y-F, Simmons BJ, Houk KN, Garg NK, J. Am. Chem. Soc 2015, 137, 4082–4085; [PubMed: 25768436] (b)Medina JM, Mackey JL, Garg NK, Houk KN, J. Am. Chem. Soc 2014, 136, 15798–15805; [PubMed: 25303232] (c)Medina JM, McMahon TC, Jiménez-Osés G, Houk KN, Garg NK, J. Am. Chem. Soc 2014, 136, 14706–14709; [PubMed: 25283710] (d)Bronner SM, Mackey JL, Houk KN, Garg NK, J. Am. Chem. Soc 2012, 134, 13966–13969; [PubMed: 22876797] (e)Im G-YJ, Bronner SM, Goetz AE, Paton RS, Cheong PH-Y, Houk KN, Garg NK, J. Am. Chem. Soc 2010, 132, 17933–17944; [PubMed: 21114321] (f)Cheong PH-Y, Paton RS, Bronner SM, Im G-YJ, Garg NK, Houk KN, J. Am. Chem. Soc 2010, 132, 1267–1269. [PubMed: 20058924]

[14]. D/IAS analysis was also performed along the reaction coordinate (i.e., at analogous geometries). The corresponding results, which are shown in the Supporting Information Part V-A, demonstrate that interaction energy controls stereoselectivity in the reaction of allene 25 and furan (24).

[15]. te Velde G, Bickelhaupt FM, Baerends EJ, Fonseca Guerra C, van Gisbergen SJA, Snijders JG, Ziegler T, J. Comput. Chem 2001, 22, 931–967.

[16]. Fonseca Guerra C, Snijders JG, te Velde G, Baerends EJ, Theor. Chem. Acc 1998, 99, 391–403.

[17]. Although experimental results for the Diels–Alder reaction of cyclohexa-1,2-diene (25) and cyclopentadiene have not been reported in the literature, we have calculated ΔG‡ for endo and exo reaction pathways. These computational results are provided in the Supporting Information Part III.

[18]. Experiments were performed with allenes 8 and 9 containing the carboxybenzyl (Cbz) group. To simplify computations, we studied allenes 31 and 34, which contain a carbomethoxy group as a surrogate for the larger Cbz group present in allenes 8 and 9.

[19]. The LUMO of the allene is expected to be more concentrated at the more electron poor **π** bond of the allene unit. See reference 2c for previously reported study of substituent effects on allene MO coefficients.

[20]. In some cases, the computed endo:exo ratios are greater than 20:1, that is that only the endo adduct is observed. Rather than provide an exact value, we represent the endo:exo ratio as “>20:1”.

[21]. See the Supporting Information Part V-C for complete D/IAS results.

[22]. Because our computational results for reaction of allene 34 and diene 39 do not quantitatively align with the experimentally observed stereoselectivity (>20:1 dr), we surveyed additional computational methods (see the Supporting Information Part VI for results). In all cases, computations predict that reaction of allene 34 and diene 39 occurs with reduced endo selectivity.

[23]. Lording WJ; Fallon T; Sherburn MS; and Paddon-Row MN The Simplest Diels–Alder Reactions are Not Endo-Selective. Chem. Sci 2020, 11, 11915–11926. [PubMed: 34123213]

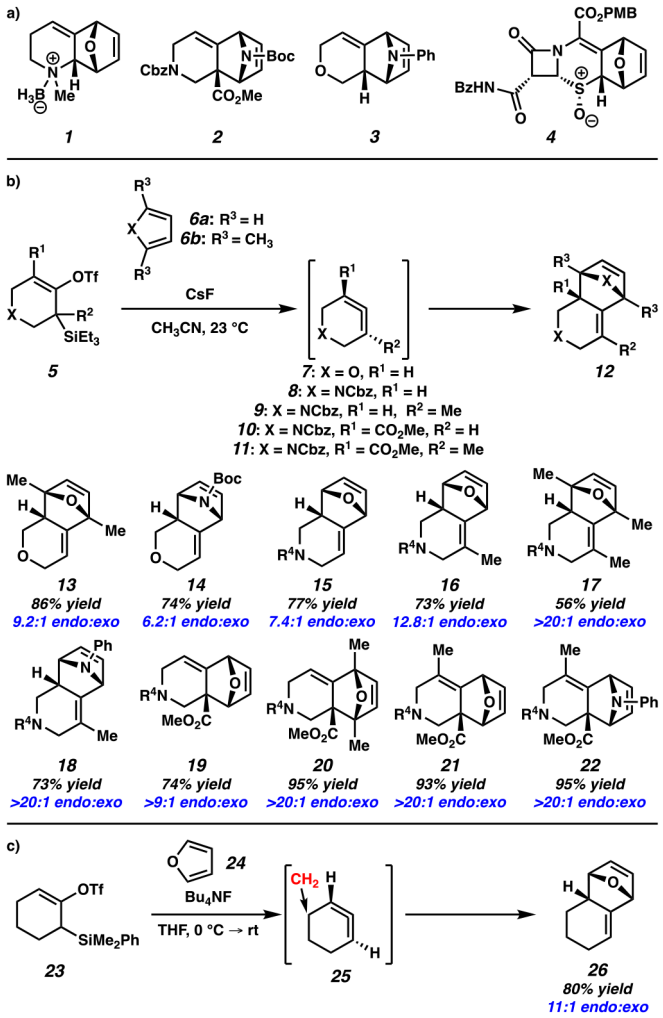

Figure 1.

a) Adducts accessible via highly *endo* selective Diels–Alder reactions of strained cyclic allenes. b) Examples of highly *endo* selective Diels-–Alder reactions with strained heterocyclic allenes. c) The *endo* selective Diels–Alder reaction of cyclohexa-1,2-diene (**25**) with furan (**24**). R^4 = carboxybenzyl.

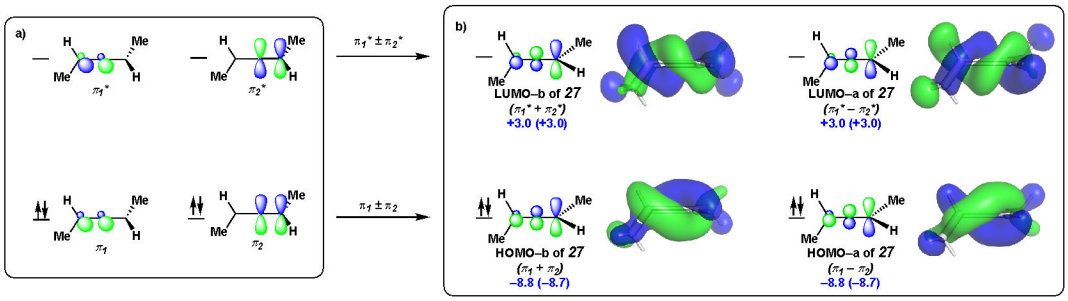

Figure 2.

a) Localized and b) Delocalized (canonical) FMOs of 2,3-pentadiene (**27**). MO structures and energies obtained with HF/6-31G(d). MO energies at the ωB97X-D/6-31G(d) level are provided in parentheses.

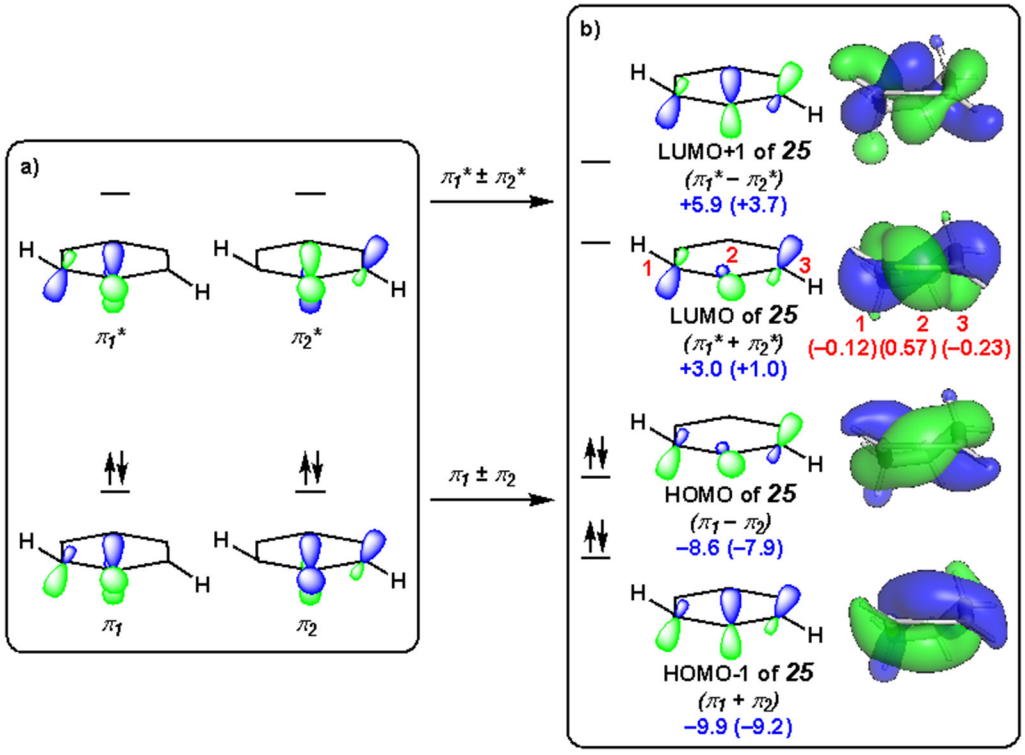

Figure 3.

a) Localized, and b) Delocalized (canonical) FMOs of cyclohexa-1,2-diene (**25**). The MO coefficients of the LUMO of **25** are shown in red. MO structures and energies obtained with HF/6-31G(d). MO energies at the ωB97X-D/6-31G(d) level are provided in parentheses.

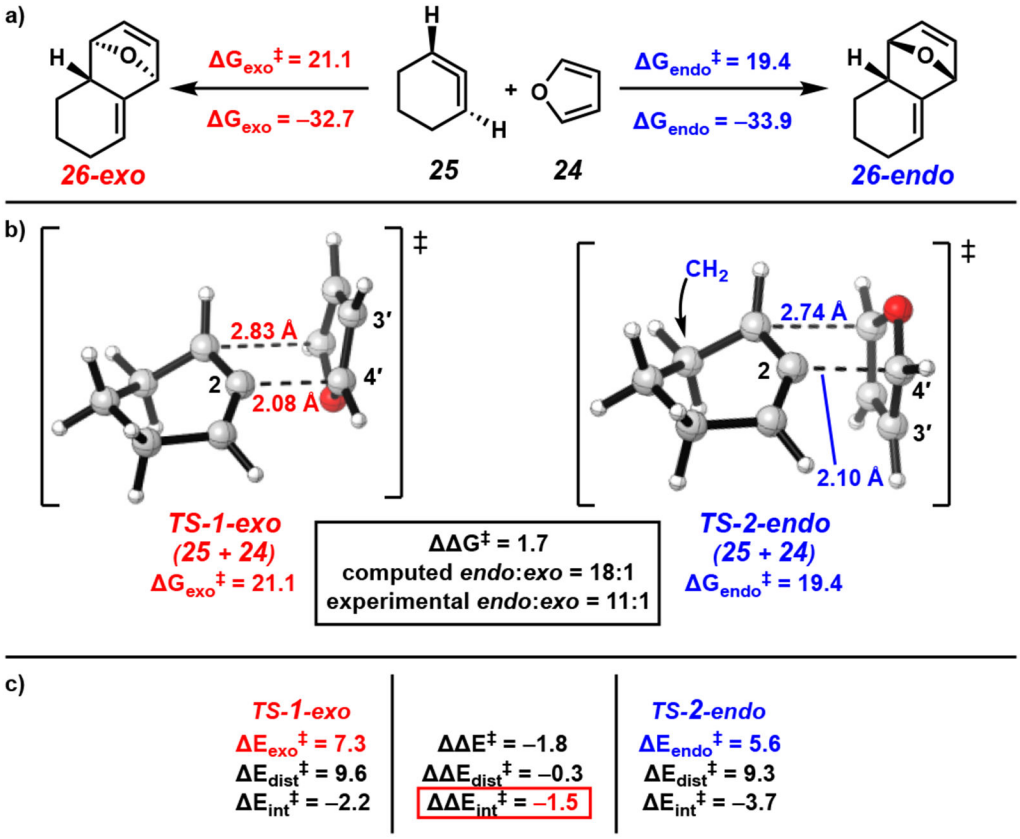

Figure 4.

a) Calculated energy barriers for *exo* and *endo* Diels–Alder reaction of cyclohexa-1,2-diene (**25**) and furan (**24**). b) *Exo* and *endo* transition state geometries. c) D/IAS analysis of *endo* and *exo* TSs. Energies in kcal mol^{-1} are for the ωB97X-D/6-311+G(d,p)/SMD(THF) level.

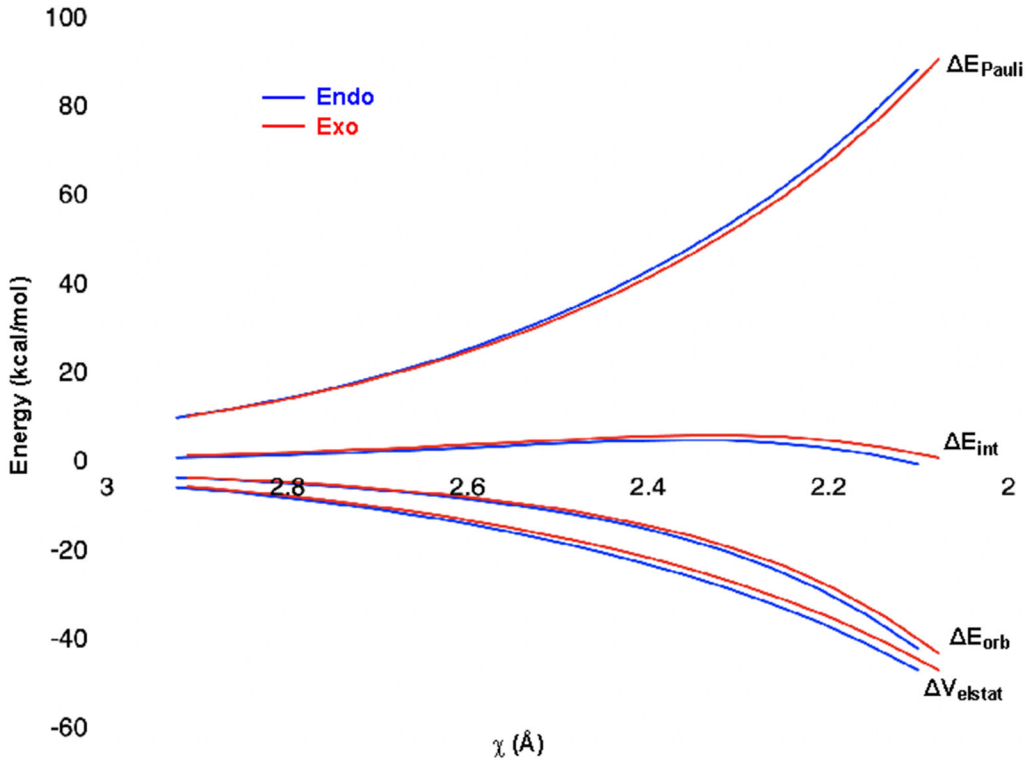

Figure 5.

EDA of the reaction of cyclohexa-1,2-diene (**25**) with furan (**24**) leading to *endo* and *exo* adducts. Energies were calculated at the ωB97X-D/TZ2P level.

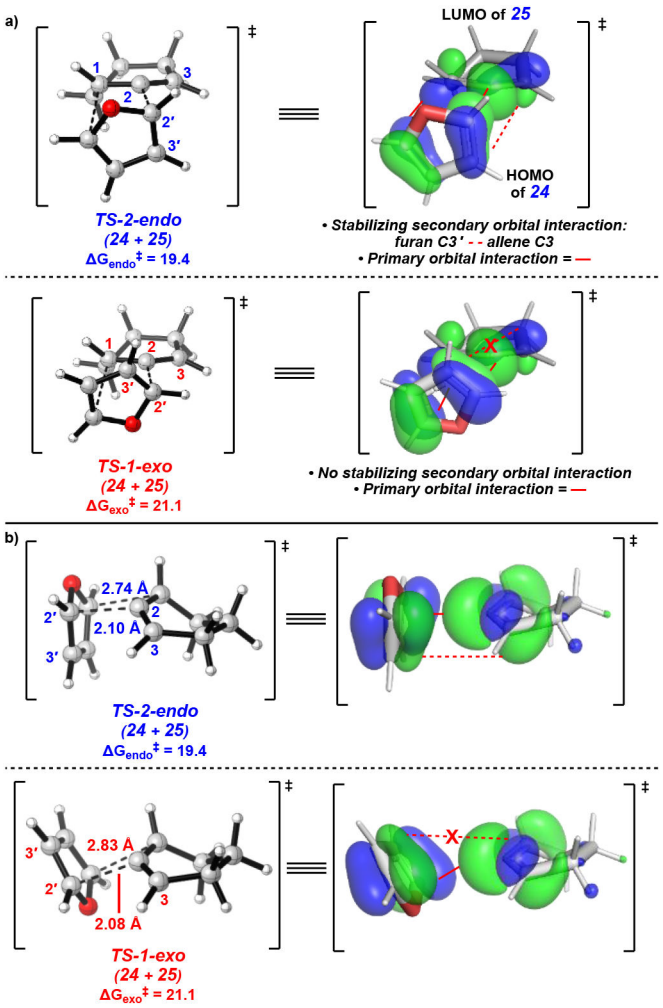

Figure 6.

HOMO furan (**24**) – LUMO allene **25** interactions in the *endo* and *exo* transition states. a) The stabilizing interaction in **TS-2-endo** is shown as the dashed red line and involves orbital overlap of the HOMO at C3' of furan (**24**) with the LUMO at C3 of **25**. This secondary orbital interaction is not present in **TS-1-exo** because the HOMO of C3' of furan (**24**) and the LUMO of C3 of **25** are out-of-phase and overlap is negligible. b) A second perspective of the orbital interactions in **TS-2-endo** and **TS-1-exo**.

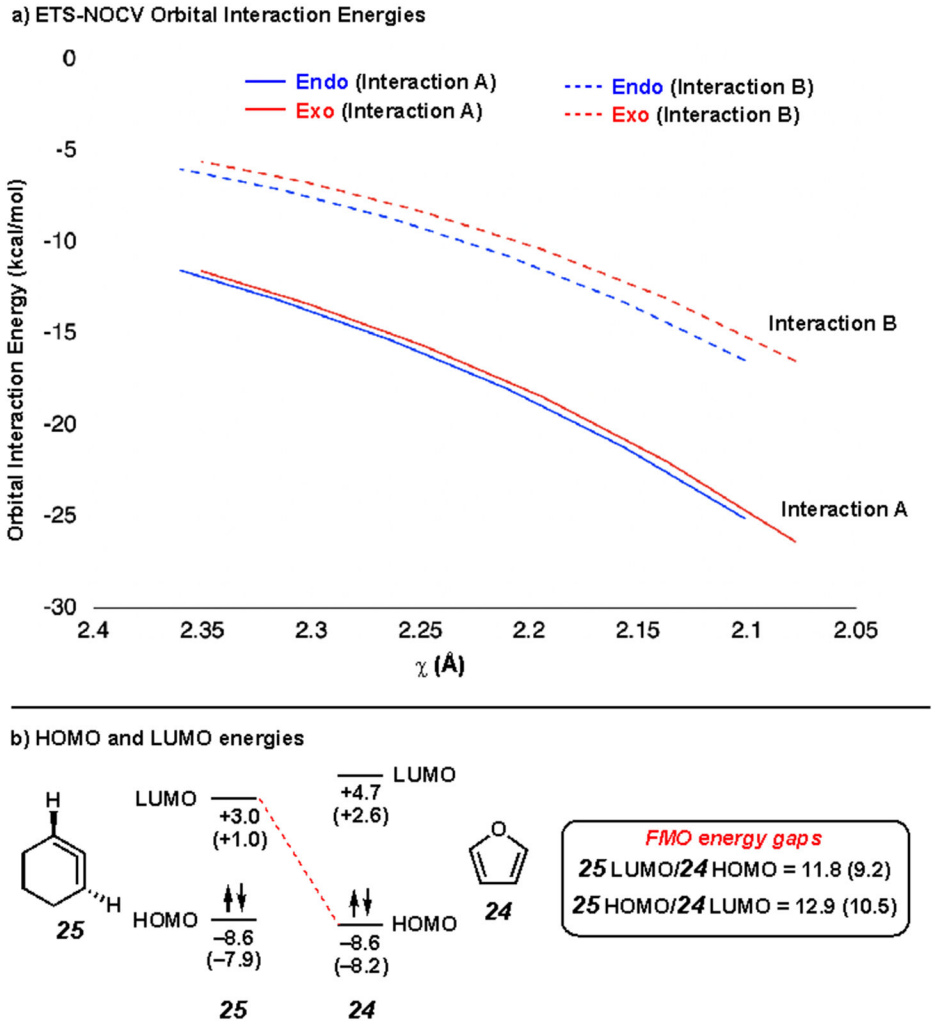

Figure 7.

a) ETS-NOCV orbital interaction energies in the Diels–Alder reaction of furan (**24**) and cyclohexa-1,2-diene (**25**) leading to *endo* and *exo* adducts (ωB97X-D/TZ2P). b) HOMO and LUMO energies of cyclohexa-1,2-diene (**25**) and furan (**24**). MO energies provided in units of eV and obtained with HF/6-31G(d). MO energies at the ωB97X-D/6-31G(d) level are provided in parentheses.

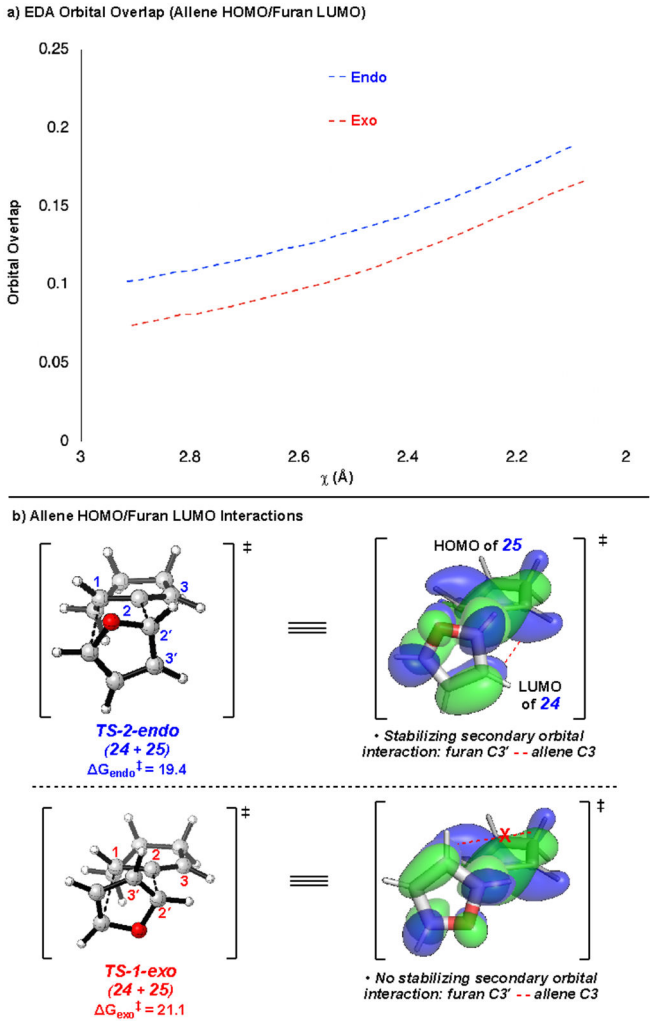

Figure 8.

a) EDA orbital overlap between the allene **25** HOMO and furan (**24**) LUMO in the Diels–Alder reaction (ωB97X-D/TZ2P). The x-axis corresponds to reaction progress or the C—C bond forming distance to the central carbon of allene **25**. b) Orbital interactions between the allene **25** HOMO and furan (**24**) LUMO in *endo* and *exo* transition states. The stabilizing interaction in **TS-2-endo** is shown as the dashed red line. In **TS-1-exo**, this interaction is antibonding and small from low overlap.

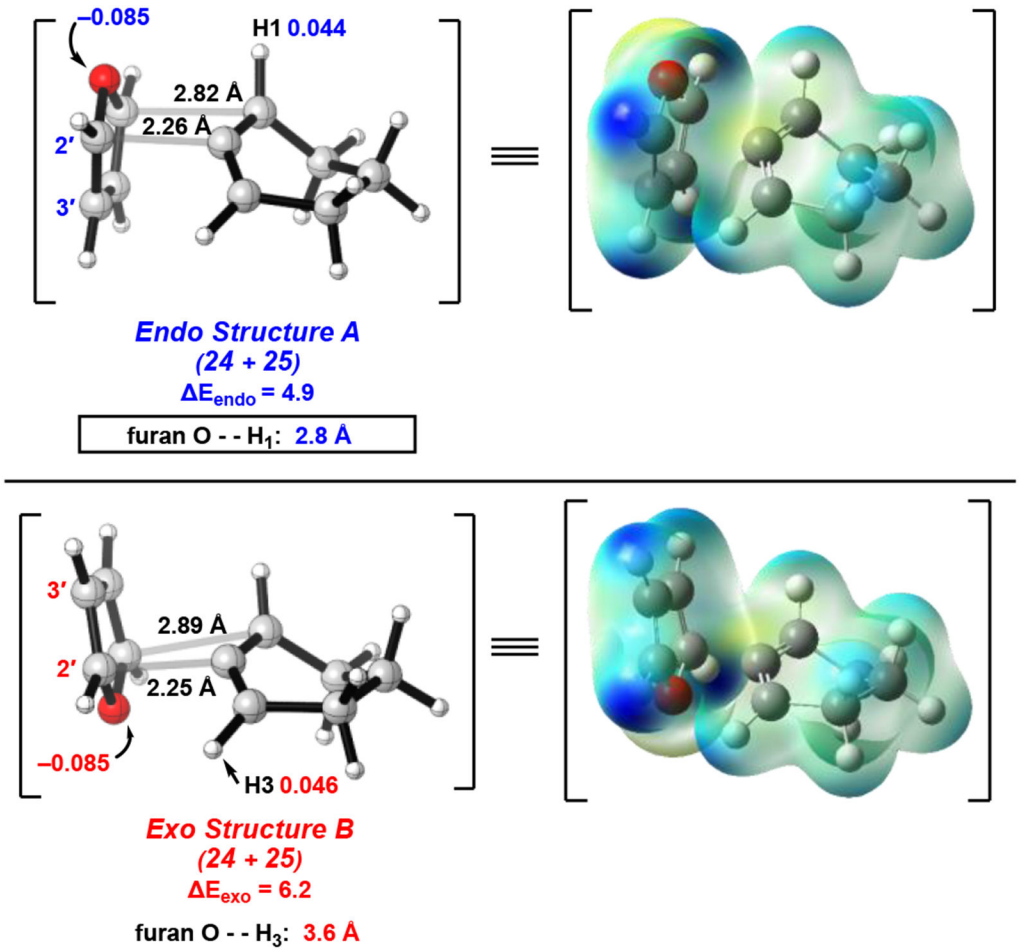

Figure 9.

Analogous geometries on the *endo* and *exo* reaction pathways of furan (**24**) and allene **25**. Hirshfeld charges and electrostatic potentials maps were calculated with ωB97X-D/6-311+G(d,p).

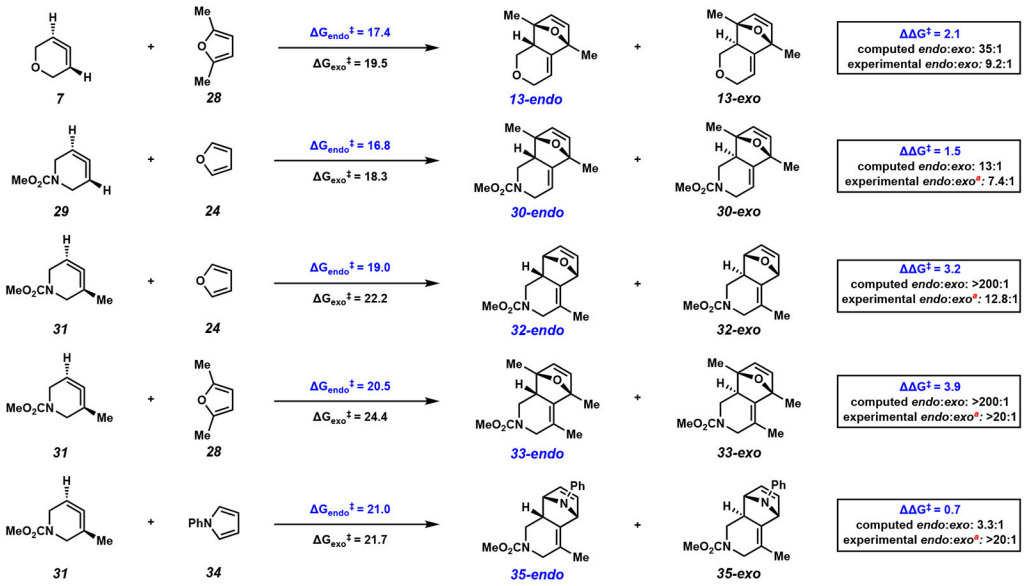

Figure 10.

Energy barriers for Diels–Alder reactions of strained heterocyclic allenes and various dienes leading to *endo* and *exo* adducts. Energies in kcal mol^{-1} computed at the ωB97X-D/6-311+G(d,p)/SMD(MeCN) level. [a]The corresponding allene derivative containing a carboxybenzyl group in place of the carbomethoxy group was used in the trapping experiment.